Holographic Molecular Binding Assays

David G. Grier[a], Rushna Quddus[b], Kaitlynn Snyder[a], and Kent Kirshenbaum[b]

[a]Department of Physics and Center for Soft Matter Research, New York University, New York, NY 10003, USA
[b]Department of Chemistry, New York University, New York, NY 10003, USA

ABSTRACT

Holographic molecular binding assays detect target molecules binding to the surfaces of specifically functionalized probe beads by measuring the associated increase in bead diameter with holographic video microscopy. Holograms of individual colloidal beads are analyzed by fitting to analytic predictions of the Lorenz-Mie theory of light scattering, yielding measurements of bead diameter with the nanometer precision required to detect binding events. Holographic binding assays share the specificity and robustness of industry-standard bead-based assays. Direct holographic readout eliminates the processing time, expense and uncertainty associated with fluorescent labeling. The underlying technology for holographic particle characterization also has a host of other applications in biopharmaceuticals, semiconductor processing and fundamental research.

Keywords: Holographic microscopy, particle characterization, label-free molecular binding assay

1. INTRODUCTION

The in-line hologram of a micrometer-scale colloidal sphere can be analyzed with predictions of the Lorenz-Mie theory of light scattering to measure the sphere's three-dimensional position with nanometer-scale precision, its refractive index to within a part per thousand, and its diameter to within a nanometer.[1,2] The key to extracting so much high-quality information is to treat hologram analysis as in inverse problem: optimizing a small set of physically relevant parameters to best account for the detailed structure of the measured hologram.[3] This approach to holographic particle characterization has applications in areas such as biopharmaceutical research and development[4] where the unique ability to differentiate particles by refractive index, and therefore by composition, can guide product formulation[5] and provides real-time feedback for process control.[6] The present contribution focuses instead on the technique's precision for measuring particle diameter, which is sufficiently fine to monitor molecules binding to the surface of a micrometer-diameter sphere. The resulting molecular binding assays share the specificity, sensitivity and flexibility of existing industry-standard bead-based assays. They offer the substantial benefit of direct holographic readout, which eliminates the cost and complexity of fluorescent labeling and detection. We have demonstrated holographic immunoassays for antibodies and antibody-based holographic binding assays for viral antigens from SARS-CoV-2 and H1N1 influenza virus.

2. HOLOGRAPHIC MOLECULAR BINDING ASSAYS

2.1 Bead-based binding assays

Figure 1(a) illustrates the core principle of bead-based molecular binding assays. Micrometer-scale probe beads are prepared by affixing molecular binding sites to their surfaces. The specificity of the assay is determined by the differential affinity of the binding site for the target molecule and for other molecules that might be present in a sample. A population of probe beads is incubated with the test sample, giving target molecules in solution a chance to find and bind to the beads' surfaces. Assuming binding to be irreversible, the fraction of occupied surface sites depends on the concentration, c, of target molecules in solution and the incubation time τ as

$$\phi(c,\tau) = 1 - \exp\left(-k_a c \tau\right), \tag{1a}$$

Further author information: (Send correspondence to D.G.G.)
D.G.G.: E-mail: david.grier@nyu.edu, Telephone: +1 (212) 998 3713

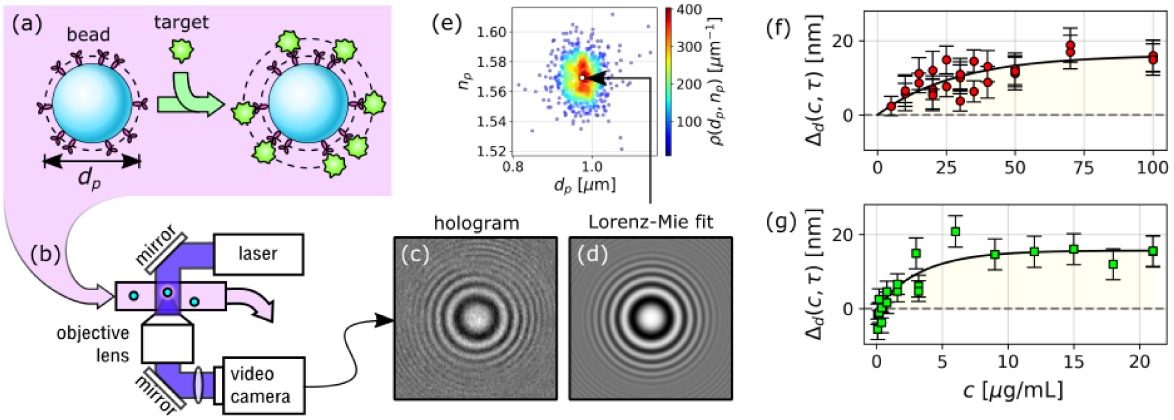

Figure 1. Holographic molecular binding assays. (a) Colloidal beads of diameter d_p are functionalized with binding sites, such as antibodies. Target molecules dispersed in the sample bind specifically to probe bead's surface, increasing its diameter. (b) The size change is detected by flowing a sample of probe beads through the observation volume of an in-line holographic microscope. (c) The hologram of an individual probe bead can be fit pixel-by-pixel to a generative model that is parameterized by d_p. (d) Optimized fit to the hologram in (c). (e) A statistical sample of single-bead measurements can be used to compute the joint distribution, $\rho(d_p, n_p)$ of observed particle diameters and refractive indexes. The population-average diameter can be determined from $\rho(d_p, n_p)$ with sub-nanometer precision. Incubating probe beads for time τ with a concentration, c, of target molecules causes the mean diameter to increase by an amount $\Delta_d(c, \tau)$. (f) Holographic assay for the antibody IgG binding to beads functionalized with protein A. (g) Holographic assay for antibody IgM.

where k_a is the rate constant for attachment. The apparent diameter of the bead, d_p, therefore increases by[7]

$$\Delta_d(c, \tau) = 2\delta\, \phi(c, \tau), \tag{1b}$$

where δ is the effective thickness of a complete monolayer of analytes, which typically ranges from a few nanometers to a few dozen nanometers.

2.2 Holographic particle characterization

As shown schematically, in Fig. 1(b), the population of probe beads conveyed by a pressure-driven flow through the observation volume of an in-line holographic microscope. Beads are illuminated by a collimated laser beam, and the light they scatter interferes with the remainder of the original beam in the focal plane of a microscope. The microscope magnifies the interference pattern and relays it to a video camera, which records its intensity. The typical hologram of a water-borne 1.5 μm-diameter silica sphere appears in Fig. 1(c).

We model the illumination as a unit-intensity monochromatic plane wave that propagates along $-\hat{z}$ with linear polarization along $\hat{x}$. The field scattered by a particle at $\mathbf{r}_p$ is roughly proportional to the field at its position and is described by the Lorenz-Mie scattering function,[8–10] $\mathbf{f}_s(k\mathbf{r})$, where k is the wavenumber of light in the medium. The intensity measured at position $\mathbf{r}$ in the focal plane therefore may be modeled as

$$b(\mathbf{r}) = \left|\hat{x} + e^{ikz_p}\, \mathbf{f}_s\left(k\left(\mathbf{r} - \mathbf{r}_p\right)\right)\right|^2. \tag{2}$$

When this generative model is applied to a uniform isotropic sphere, the computed intensity, $b(\mathbf{r})$, is parameterized by the sphere's three-dimensional position, $\mathbf{r}_p$, its refractive index, n_p, and its diameter, d_p. The computed hologram in Fig. 1(d) was obtained by optimizing these five values for best agreement with the measured intensity pattern in Fig. 1(c).

Each point of the scatter plot in Fig. 1(e) represents the measured diameter and refractive index for one bead in a sample of 1000 particles. These data were acquired with a commercial instrument for holographic particle characterization (Spheryx, Inc., xSight) operating at a vacuum wavelength of 447 nm. The points are colored according to the local density of observations, $\rho(d_p, n_p)$. The probe beads consist of 1 μm-diameter polystyrene spheres with a covalently linked coating of protein A (Bangs Laboratories, CP02000). The width of the measured size distribution is dominated by the actual spread of values in the sample. The center of the distribution can

be determined with sub-nanometer precision.[11,12] Multiple single-particle measurements can be performed per second[13–15] so that a statistical sample such as the example in Fig 1(d) can be amassed in under 10 min.

2.3 Label-free holographic molecular binding assays

Comparing population averages before and after incubation for time τ yields a value for the change in the beads' apparent diameter, $\Delta_d(c,\tau)$, that can be used to analyze the binding process. Figure 1(f) shows typical results for the antibody immunoglobulin G (IgG) binding to beads that are functionalized with protein A, a pathogen-derived product that specifically and strongly binds antibodies. Each point represents one differential measurement performed after the probe beads were incubated with a known antibody concentration for $\tau = 45$ min.

A comparable incubation time would be required for any binding assay. Standard assays then require a second incubation with fluorescent labels to ascertain whether or not target molecules have been immobilized on the bead surfaces. This labeling step not only doubles an assay's processing time, but requires specialized reagents whose development time can delay deployment of novel assays. The challenge of quantitating labeled beads' fluorescence contributes to uncertainty in the assay's interpretation. Holographic particle characterization, by contrast, yields results for $\Delta_d(c,\tau)$ directly and thus is a label-free readout mechanism.

The solid curve in Fig. 1(f) is a two-parameter fit to Eq. (1) for the effective layer thickness $\delta = (8.0 \pm 0.5)$ nm and the kinetic rate constant, $k_a = (1.8 \pm 0.5) \times 10^3\,\mathrm{M}^{-1}\,\mathrm{s}^{-1}$, which is consistent with results from orthogonal measurements based on surface-plasmon resonance detection.[16] Holographic readout has the advantage over these techniques that its probe beads can be synthesized in bulk without requiring microfabrication.

Figure 1(g) presents comparable results for the antibody IgM binding to probe beads functionalized with protein A. The rate constant in this case is $k_a = (2.5 \pm 0.8) \times 10^5\,\mathrm{M}^{-1}\,\mathrm{s}^{-1}$, which reflects the substantially greater activity of IgM and is consistent with its role as a first line of defense in the immune system. Control measurements performed by replacing antibodies with alcohol dehydrogenase, a protein of comparable size, show no shift in $\Delta_d(c,\tau)$.

2.4 Effective-medium interpretation

The layer thickness, δ, is not simply related to the size of a target molecule because the Lorenz-Mie model for light scattering treats the coated sphere as if it were homogeneous and the molecular coating generally has a different refractive index from the substrate bead. Gaps between bound target molecules, furthermore, are filled by the fluid medium, which further modifies the refractive index. Rather than modeling the influence of a multicomponent molecular coating on light scattering by a micrometer-diameter sphere, we instead interpret results of the straightforward Lorenz-Mie analysis using Maxwell Garnett effective-medium theory.[17] Numerical studies[7] confirm that the change in bead diameter obtained from this effective-sphere interpretation is proportional to the fractional coverage of bound target molecules, and therefore that Eq. (1) is valid for these data. The effective layer thickness, δ, not only depends on the molecules' physical size but also on the refractive indexes of the substrate bead, the bound molecules and the medium. This means that the sensitivity of the binding assay can be optimized by choosing appropriate material parameters with the largest values of δ being obtained for substrate beads that are most nearly index-matched to the medium.[7] Replacing polystyrene substrate spheres with silica spheres, for example, increases the effective layer thickness for the immunoassays presented in Fig. 1 from $\delta = 8$ nm to $\delta = 15$ nm and thereby improves the assays' sensitivity.

3. DISCUSSION

Holographic video microscopy provides the basis for a novel class of label-free bead-based molecular binding assays. Using functionalized probe beads to immobilize target molecules ensures the assays' selectivity. The excellent size resolution afforded by holographic particle characterization ensures their sensitivity. By eliminating fluorescent labeling, holographic assays are easier to develop and faster and cheaper to run than conventional bead-based assays. Interpreting results with effective-medium theory minimizes computational complexity while providing opportunities to optimize sensitivity and throughput. Holographic characterization also is compatible with optical manipulation techniques, such as holographic optical trapping, which creates additional opportunities for single-bead holographic assays, including optically-multiplexed arrays for differential medical diagnostic testing.

ACKNOWLEDGMENTS

This work was funded primarily by the National Science Foundation under Awards DMR-2027013 and DMR-2104837 in part by the National Institutes of Health SBIR program of the National Institutes of Health under Award No. R44TR001590. The Spheryx xSight used for this study was purchase by the NYU MRSEC as shared instrumentation under NSF Award No. DMR-1420073. The Titan Xp and Titan RTX GPUs used for this work were provided by GPU Grants from NVIDIA. The custom holographic characterization instrument was constructed with support from the MRI program of the NSF under Award Number DMR-0922680 and is maintained by NYU's Center for Soft Matter Research as shared instrumentation.

REFERENCES

[1] Lee, S.-H., Roichman, Y., Yi, G.-R., Kim, S.-H., Yang, S.-M., van Blaaderen, A., van Oostrum, P., and Grier, D. G., "Characterizing and tracking single colloidal particles with video holographic microscopy," *Opt. Express* **15**, 18275–18282 (2007).

[2] Krishnatreya, B. J., Colen-Landy, A., Hasebe, P., Bell, B. A., Jones, J. R., Sunda-Meya, A., and Grier, D. G., "Measuring Boltzmann's constant through holographic video microscopy of a single sphere," *Am. J. Phys.* **82**, 23–31 (2014).

[3] Martin, C., Altman, L. E., Rawat, S., Wang, A., Grier, D. G., and Manoharan, V. N., "In-line holographic microscopy with model-based analysis," *Nature Reviews Methods Primers* **2**, 83 (2022).

[4] Winters, A., Cheong, F. C., Odete, M. A., Lumer, J., Ruffner, D. B., Mishra, K. I., Grier, D. G., and Philips, L. A., "Quantitative differentiation of protein aggregates from subvisible contaminants in viscous mixtures through holographic characterization," *J. Pharm. Sci.* **109**, 2405–2412 (2020).

[5] Rahn, H., Oeztuerk, M., Hentze, N., Junge, F., and Hollmann, M., "The strengths of total holographic video microscopy in detecting sub-visible protein particles in biopharmaceuticals: A comparison to Flow Imaging and Resonant Mass Measurement," *J. Pharm. Sci.* (2022).

[6] Wang, C., Moyses, H. W., and Grier, D. G., "Stimulus-responsive colloidal sensors with fast holographic readout," *Appl. Phys. Lett.* **107**, 051903 (2015).

[7] Altman, L. E. and Grier, D. G., "Interpreting holographic molecular binding assays with effective medium theory," *Biomed. Opt. Express* **11**, 5225–5236 (2020).

[8] Bohren, C. F. and Huffman, D. R., [*Absorption and Scattering of Light by Small Particles*], Wiley Interscience, New York (1983).

[9] Mishchenko, M. I., Travis, L. D., and Lacis, A. A., [*Scattering, Absorption and Emission of Light by Small Particles*], Cambridge University Press, Cambridge (2001).

[10] Gouesbet, G. and Gréhan, G., [*Generalized Lorenz-Mie Theories*], Springer-Verlag, Berlin (2011).

[11] Zagzag, Y., Soddu, M. F., Hollingsworth, A. D., and Grier, D. G., "Holographic molecular binding assays," *Scientific Reports* **10**, 1932 (2020).

[12] Snyder, K., Quddus, R., Hollingsworth, A. D., Kirshenbaum, K., and Grier, D. G., "Holographic immunoassays: Direct detection of antibodies binding to colloidal spheres," *Soft Matter* **16**, 10180–10186 (2020).

[13] Cheong, F. C., Krishnatreya, B. J., and Grier, D. G., "Strategies for three-dimensional particle tracking with holographic video microscopy," *Opt. Express* **18**, 13563–13573 (2010).

[14] Altman, L. E. and Grier, D. G., "CATCH: Characterizing and Tracking Colloids Holographically using deep neural networks," *J. Phys. Chem. B* **124**, 1602–1610 (2020).

[15] Altman, L. E. and Grier, D. G., "Machine learning enables precise holographic characterization of colloidal materials in real time," *Soft Matter* , submitted for publication (2022).

[16] Saha, K., Bender, F., and Gizeli, E., "Comparative study of igg binding to proteins g and a: nonequilibrium kinetic and binding constant determination with the acoustic waveguide device," *Anal. Chem.* **75**(4), 835–842 (2003).

[17] Markel, V., "Introduction to the Maxwell Garnett approximation: tutorial," *J. Opt. Soc. Am. A* **33**, 1244–1256 (2016).